CHAPTER 10

Postcapture Attitude Control for a TSR-Target Combination System

The attitude control of a tethered system in space has been investigated by many researchers. Nohmi [1–3] proposed a control scheme using the arm link to regulate the TSR's attitude during the deployment phase, and a microgravity experiment was carried out to validate the feasibility of this scheme. Godard et al. [4] presented a nonlinear optimal controller based on inverse optimal technique to control the attitude of a satellite via tether offset variations. The attitude of the mother satellite is regulated by four tethers, which are connected with the subsatellite as described in the literature [5]. Beda [6] investigated how the attitude dynamics of a tethered satellite can be controlled for eccentric orbits by simply using the feedback of the pitch angle. The tether tension/length control law was designed to control the attitude of a tethered satellite formation as described in the literature [7]. Chang et al. [8] analyzed the attitude dynamics and control of a three-inline tethered satellite flying formation, and the state-dependent Riccati equation controller was used to regulate the attitude errors. By using two passive dampers placed at the tether attachment point, Menon and Bombardelli [9] proposed a method to control the position and attitude of the two tethered units. Bergamaschi and Bonon [10] studied the coupling between the tether taut string vibrations and the satellite attitude motion.

The capture and postcapture control is one of the most important problems for the traditional space robot that has been studied by many researchers. Yoshida et al [11] proposed a possible control sequence that included the bias momentum approach during the approaching phase, the impedance control during the impact phase and the distributed momentum control during the postimpact phase for a successful capturing operation. Flores-Abad and Ma [12] proposed an optimal control strategy for a space manipulator to provide minimal impact to the base satellite during a capturing operation. Liu et al. [13] derived an impact model to simulate the post-impact dynamics of the entire systems and designed a PD controller to maintain the stabilization of the robot system after the capture of the object.

Tethered Space Robot
https://doi.org/10.1016/B978-0-12-812309-6.00010-5

Nguyen-Huynh and Sharf [14] presented a trajectory generation algorithm for a space manipulator after capturing an uncooperative tumbling target. Aghili [15,16] focused on controlling the space manipulator in the postcapture phase to bring a tumbling satellite to rest. Xu et al. [17] proposed a method for berthing a target and reorientating the base using manipulator motion only after the capture.

Also, Nakamura et al. [18] used the tension and thruster to realize the collaborative control of the tethered space robot during the approaching target phase. Spencer [19] compared the dynamics and control of a space robot subjected to a tether tension force with those for a free-floating space robot.

In the postcapture phase, the gripper and the target form a new combination system. The dynamic characteristics of this combination system are different from those of a TSR in its deployment, approach, or capture phase. Due to the presence of the space tether, the postcapture dynamic characteristics of the combination system can be distinguished from the aforementioned characteristics of a traditional space robot. The collision during the capture and the original target rotation of the target lead to a tumbling combination, which could cause the tether to become tangled with the combination and even influence the security of the space platform.

The attitude control of the combination can hardly be achieved by the thrusters of the gripper alone, because the control torque of the thrusters and the fuel of the gripper are limited. In the existing literature, the tether is usually used to provide the tension to control the relative positions of the satellite formation or the positions of the space robots during the phase of release toward the target. However, the space tether can also provide great control torques for the attitude control. Therefore this chapter aims to design an attitude-coordinated controller of the tether and the thrusters to stabilize the tethered space robot-target combination system and reduce the fuel consumption at the same time.

10.1 DYNAMICS MODEL

As shown in Fig. 10.1, in the postcapture phase, the gripper rotates along with the target after the capture, and the combination system consists of the gripper and the target. The origin of the platform orbital frame, $Ox_py_pz_p$, is located at the centroid of the space platform. The axes of the coordinate are oriented as follows: the x-axis is in the orbital plane in the local horizontal direction, the y-axis is along the orbital normal, and the z-axis is collinear with a line that extends from the center of the Earth to the centroid of

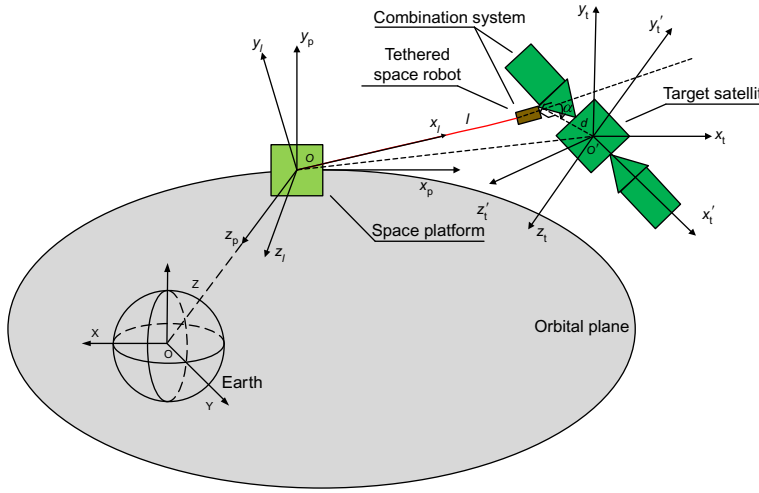

Fig. 10.1 Target capture of the TSR.

the space platform and completes a right-handed triad. Given the flying-around distance for the platform, observing the target before the capturing mission, and the limited fuel of the gripper for the capturing mission, the tether is assumed to be a few hundreds of meters long in this study. Therefore the $Ox_t y_t z_t$ denotes the combination orbital frame that is approximately parallel with $Ox_p y_p z_p$. The $Ox_l y_l z_l$ is the tether frame with its x-axis along the tether direction, and $Ox_t' y_t' z_t'$ is the combination body frame.

The following assumptions are made:

(1) The tether is assumed to be inelastic and massless. Compared with space platform or robot-target combination at hundreds or thousands of kilograms level, the mass of the tether at hundreds of meters level is relatively small and could be neglected. For example, the density of the Kevlar tether [20] (1 mm diameter) used for ESA's ROGER project is 4.5 kg/km, and the mass of 1 km tether here is only 4.5 kg. Therefore the influence of the tether to the issue discussed herein can be neglected and the tether is assumed to be massless.

(2) No time delay exists in the tension transmission along the space tether and force feedback of tether reel, and the vibration of the space tether is neglected. Moreover, no tension exists when the space tether is slack.

(3) The target is firmly captured with no sway of the solar paddle or other unstable phenomena occurring during the attitude control.

(4) The platform can overcome the influence of a tether tension by its own thrusters, and its position and attitude can be maintained during the coordinated attitude control of the combination system.

10.1.1 Attitude Dynamics Model

The combination system is assumed to be a rigid body, attitude dynamic equation of which can be given by the following equation:

$$\boldsymbol{J}\dot{\boldsymbol{\omega}} = -\boldsymbol{\omega}^{\times}\boldsymbol{J}\boldsymbol{\omega} + \boldsymbol{T}_c + \boldsymbol{T}_l + \boldsymbol{T}_l + \boldsymbol{T}_d \tag{10.1}$$

where $\boldsymbol{\omega} = [\omega_1 \quad \omega_2 \quad \omega_3]^T \in R^3$ denotes the absolute angular velocity of the combination expressed in the body frame $Ox_t'y_t'z_t'$, $\boldsymbol{J} \in R^{3\times3}$ is the inertia matrix of the combination and $\boldsymbol{J} = \boldsymbol{J}_0 + \Delta\boldsymbol{J}$ with $\boldsymbol{J}_0$ as the nominal value and $\Delta\boldsymbol{J}$ is the bounded uncertainty due to the thruster consumption; $\boldsymbol{T}_c \in R^3$ denotes the control torque of the gripper and is equivalently realized via PWM thrusters. $\boldsymbol{T}_l \in R^3$ denotes the control torque of the tether, and $\boldsymbol{\omega}^{\times}$ is the skew-symmetric matrix of $\boldsymbol{\omega}$.

$\boldsymbol{T}_d \in R^3$ is the attitude disturbance torque caused by the thruster force of the gripper. The target is assumed to have no capacity for orbit control, and the gripper's thrusters are utilized to control the combination orbit. The gripper is not located in the centroid of the combination and the vector of the control force does not extend through the centroid of the combination; Therefore $\boldsymbol{T}_d$ is generated.

The MPR [21] are used to describe the kinematics model of the combination attitude as follows:

$$\dot{\boldsymbol{\sigma}} = G(\boldsymbol{\sigma})\boldsymbol{\omega} \tag{10.2}$$

where $\boldsymbol{\sigma} = [\sigma_1 \quad \sigma_2 \quad \sigma_3]^T \in R^3$ and $G(\boldsymbol{\sigma})$ is defined as follows:

$$G(\boldsymbol{\sigma}) = \frac{1}{4}\left[\left(1 - \boldsymbol{\sigma}^T\boldsymbol{\sigma}\right)\boldsymbol{I} + 2\boldsymbol{\sigma}^{\times} + 2\boldsymbol{\sigma}\boldsymbol{\sigma}^T\right] \tag{10.3}$$

where $\boldsymbol{I}$ is a 3×3 unit matrix.

The transformation matrix from the platform orbital frame to the combination body frame is:

$$\boldsymbol{R} = \boldsymbol{I}_3 - \frac{4(1-\boldsymbol{\sigma}^2)}{(1+\boldsymbol{\sigma}^2)^2}[\boldsymbol{\sigma}^{\times}] + \frac{8}{(1+\boldsymbol{\sigma}^2)^2}[\boldsymbol{\sigma}^{\times}]^2 \tag{10.4}$$

Define the transformation matrix from the platform orbital frame to the tether frame as $\boldsymbol{R}_{lp}$, then the transformation matrix $\boldsymbol{R}_{bl}$ from the tether frame $Ox_ly_lz_l$ to the combination body frame $Ox_t'y_t'z_t'$ is given by:

$$\boldsymbol{R}_{bl} = \boldsymbol{R}\boldsymbol{R}_{lp}^{-1} \tag{10.5}$$

For simplicity, the relative attitude angles from the tether frame $Ox_l y_l z_l$ to the combination body frame $Ox_t' y_t' z_t'$ are described by the Euler angles, including the roll angle ϕ, the pitch angle θ, and the yaw angle ψ of the 1-2-3 Euler rotation sequence. The term $\boldsymbol{R}_{bl}$ can be expressed by ϕ, θ, and ψ as follows:

$$\boldsymbol{R}_{bl} = \begin{bmatrix} \cos\psi\cos\theta & \cos\psi\sin\theta\sin\phi + \sin\psi\cos\phi & -\cos\psi\sin\theta\cos\phi + \sin\psi\sin\phi \\ -\sin\psi\cos\theta & -\sin\psi\sin\theta\sin\phi + \cos\psi\cos\phi & \sin\psi\sin\theta\cos\phi + \cos\psi\sin\phi \\ \sin\theta & -\cos\theta\sin\phi & \cos\theta\cos\phi \end{bmatrix} \tag{10.6}$$

Combine Eqs. (10.5) and (10.6), and the three Euler angles ϕ, θ, and ψ can be obtained.

$$\begin{cases} \theta = \arcsin\left(\boldsymbol{R}_{bl}(3,1)\right) \\ \phi = \arctan\left(-\dfrac{\boldsymbol{R}_{bl}(3,2)}{\boldsymbol{R}_{bl}(3,3)}\right) \\ \psi = \arctan\left(-\dfrac{\boldsymbol{R}_{bl}(2,1)}{\boldsymbol{R}_{bl}(1,1)}\right) \end{cases} \tag{10.7}$$

The error attitude MRP σ_e and the error attitude angular velocity $\boldsymbol{\omega}_e$ of the body frame are defined as follows [22]:

$$\begin{cases} \sigma_e = \sigma \otimes {\sigma_d}^{-1} \\ \boldsymbol{\omega}_e = \boldsymbol{\omega} - \boldsymbol{\omega}_d \end{cases} \tag{10.8}$$

where $\boldsymbol{\omega}_d$ denotes the desired angular velocity in the body frame and σ_d the desired attitude. The symbol $\otimes$ denotes the MRP multiplication, which can be defined as follows:

$${\sigma_1} \otimes {\sigma_2}^{-1} = \frac{\left(1 - {\sigma_2}^T\sigma_2\right)\sigma + \left(\sigma_1^T\sigma_1 - 1\right)\sigma_2 - 2\sigma_2 \times \sigma_1}{1 + \left(\sigma_2^T\sigma_2\right)\left(\sigma_1^T\sigma_1\right) + 2\sigma_2^T\sigma_1} \tag{10.9}$$

Substitute Eq. (10.8) into (10.1), and the error attitude dynamic equation and the kinematics equation can be obtained:

$$\begin{cases} \dot{\sigma}_e = G(\sigma_e)\boldsymbol{\omega}_e \\ \boldsymbol{J}\dot{\boldsymbol{\omega}}_e = -\boldsymbol{\omega}^{\times}\boldsymbol{J}\boldsymbol{\omega} - \boldsymbol{J}\boldsymbol{R}\dot{\boldsymbol{\omega}}_d + \boldsymbol{T}_c + \boldsymbol{T}_l + \boldsymbol{T}_d \end{cases} \tag{10.10}$$

10.1.2 Orbit Dynamic Model

The orbit motion of the combination system can be described by the Hill equation as follows:

$$\begin{cases} \ddot{x} - 2n\dot{z} = a_x + a_{tx} - n^2\varepsilon_x \\ \ddot{y} + n^2 y = a_y + a_{ty} - n^2\varepsilon_y \\ \ddot{z} + 2n\dot{x} - 3n^2 z = a_z + a_{tz} - n^2\varepsilon_z \end{cases} \tag{10.11}$$

where $[x \;\; y \;\; z]^T \in R^3$ is the centroid position of the combination in the platform orbital frame $Ox_py_pz_p$, n denotes the mean orbital angular velocity. $[a_x \;\; a_y \;\; a_z]^T \in R^3$ denotes the linear acceleration of the gripper's thruster force, and $[a_{tx} \;\; a_{ty} \;\; a_{tz}]^T \in R^3$ denotes the linear acceleration due to the tether tension. Assuming the target has no orbital control capacity, the orbit of the combination system can only be controlled by the thrusters of the gripper or possibly by the thrusters and the tether tension together.

Define the position vector of the capture position in the combination body frame as $\boldsymbol{d}$, and the tether tension as F_l. A tether tension that is too great can strongly influence the space platform and even cause instability throughout the system; therefore F_l should satisfy the following constraint:

$$F_l \le F_{l\max} \tag{10.12}$$

Hence, the tether tension vector in the platform frame $Ox_py_pz_p$ can be written as:

$$\boldsymbol{F} = -\frac{[x, y, z]^T + \boldsymbol{R}^{-1}\boldsymbol{d}}{\left\|[x, y, z]^T + \boldsymbol{R}^{-1}\boldsymbol{d}\right\|} F_l \tag{10.13}$$

The linear accelerations of the tether tension are given by:

$$[a_{tx} \;\; a_{ty} \;\; a_{tz}]^T = -\frac{[x, y, z]^T + \boldsymbol{R}^{-1}\boldsymbol{d}}{\left\|[x, y, z]^T + \boldsymbol{R}^{-1}\boldsymbol{d}\right\|} \cdot \frac{F_l}{m} \tag{10.14}$$

where m is the mass of the combination system.

By multiplying by the transformation matrix $\boldsymbol{R}$, the tether force in the combination body frame can be obtained, and the tether control torque can be acquired:

$$\boldsymbol{T}_l = \boldsymbol{d} \times (\boldsymbol{R}\boldsymbol{F}) \tag{10.15}$$

10.1.3 Dynamic Analysis

The gripper rotates together with the target after the capture. The thruster force of the gripper and the tension along the space tether are used to control

the combination attitude. By setting the left side of Eq. (10.15), $\boldsymbol{T}_l$, to be zero yields the following:

$$(\boldsymbol{RF}) \times \boldsymbol{d} = \boldsymbol{0}$$

The equation above suggests that the tether torque has no influence on the combination attitude when the tether vector is collinear with $\boldsymbol{d}$. The corresponding attitude is chosen as the desired attitude $\boldsymbol{\sigma}_d = [\sigma_{d1} \quad \sigma_{d2} \quad \sigma_{d3}]^T$. This definition has remarkable advantages; if the desired states are not $\boldsymbol{\sigma}_d$, the combination will sway and even become unstable when retrieved due to the tether tension torque or deorbited to another orbit after the combination attitude is stabilized. The value of $\boldsymbol{\sigma}_d$ changes with the position of the combination system and can be deduced as follows:

The unit vector of the tether vector in the platform orbital frame is $\dfrac{[x, y, z] + \boldsymbol{R}^{-1}\boldsymbol{d}}{\left\|[x, y, z] + \boldsymbol{R}^{-1}\boldsymbol{d}\right\|}$. When the desired attitude is obtained, the tether frame $Ox_l y_l z_l$ is parallel to the combination body frame $Ox_t' y_t' z_t'$, and the orientation of the tether follows the Ox_t' axis. The unit vector of the tether in the tether frame is $[1, 0, 0]^T$, and the transformation matrix from the platform to the tether frame is R_{lp}, then the following relationship is satisfied:

$$[1, 0, 0]^T = \boldsymbol{R}_{lp} \frac{[x, y, z]^T + \boldsymbol{R}^{-1}\boldsymbol{d}}{\left\|[x, y, z]^T + \boldsymbol{R}^{-1}\boldsymbol{d}\right\|} \tag{10.16}$$

Equating Eq. (10.16) yields:

$$\boldsymbol{R}_{lp} = [1, 0, 0]^T \left(\frac{[x, y, z]^T + \boldsymbol{R}^{-1}\boldsymbol{d}}{\left\|[x, y, z]^T + \boldsymbol{R}^{-1}\boldsymbol{d}\right\|} \right)^+ \tag{10.17}$$

where $(\cdot)^+$ denotes the Moore-Penrose inverse.

From the transformation matrix $\boldsymbol{R}_{lp}$, the rotating angle α, and the Euler axis $\boldsymbol{e} = (e_x \quad e_y \quad e_z)^T$ are given by:

$$\begin{cases} \cos\alpha = \left(\boldsymbol{R}_{lp11} + \boldsymbol{R}_{lp22} + \boldsymbol{R}_{lp33} - 1\right)/2 \\ e_x = \left(\boldsymbol{R}_{lp23} - \boldsymbol{R}_{lp32}\right)/(2\sin\alpha) \\ e_y = \left(\boldsymbol{R}_{lp31} - \boldsymbol{R}_{lp13}\right)/(2\sin\alpha) \\ e_z = \left(\boldsymbol{R}_{lp12} - \boldsymbol{R}_{lp21}\right)/(2\sin\alpha) \end{cases} \tag{10.18}$$

According to the definition of the MRP, $\boldsymbol{\sigma}_d$ is obtained as follows:

$$\boldsymbol{\sigma}_d = \tan\frac{\alpha}{4}\boldsymbol{e} \tag{10.19}$$

Also, the desired angular velocity is defined as: $\boldsymbol{\omega}_d = [0 \quad 0 \quad 0]^T$.

10.2 COORDINATED CONTROL STRATEGIES

After the capture of the target, using the traditional thruster control alone to stabilize the combination attitude can lead to the following cases:

(1) The combination attitude cannot be stabilized quickly because the control torque of the gripper is limited with the consideration of the mass of the combination, and the tether may eventually become intertwined with the combination. This serious situation is rather dangerous and the platform could even be threatened due to the existence of the space tether.

(2) Even the combination attitude can be stabilized by the thruster control, but the fuel consumption will be too great.

As a result, the attitude control of the tethered space robot-target combination can hardly be achieved by the traditional thruster control alone, causing the fuel consumption of the thruster control alone to be too great. Considering that the tether could provide considerable control torque, the design of the attitude coordinated controller using the tether tension and the thruster force is discussed in this study. The tether tension could lead to a change in the combination position; however, the attitude control is more urgent and important than the position control because a spinning of the combination will cause the tether to become intertwined and can even cause instabilities of the platform and the entire system, whereas a change in the position of the combination does not have a great influence.

The chosen desired attitude $\boldsymbol{\sigma}_d$ varies with the combination position, and the position control will not be discussed here. Furthermore, the combination position is assumed to be without control for simplicity and convenience of the attitude controller design; therefore, $\boldsymbol{T}_d$ and $\begin{bmatrix} a_{tx} & a_{ty} & a_{tz} \end{bmatrix}^T$ are set to zero.

The inertial matrix and the centroid position of the combination system are as yet unknown. Therefore the parameters should be identified prior to the controller design. Considering the attitude characteristics of the combination, the coordinated controller is designed to consist of two attitude controllers, which are used according to the switching conditions. During the initial stage of the attitude control, the pitch and yaw motion of the combination are controlled via tether because the space tether can provide greater torque than the gripper thrusters. Meanwhile, the roll motion is controlled by the thruster. The attitudes of the three axes are primarily controlled by the tether tension and the thruster. When the pitch and yaw attitude are stabilized within a certain range, the controller is switched to the

thruster control only because the smaller pitch and yaw angles lead to a smaller torque arm, and greater tether tension is necessary to obtain the required torque. Greater tether tension will have a greater influence over the position of the combination; thus an increased tether tension is unfeasible and should be avoided. Moreover, the thruster control could achieve high-accuracy attitude control, which is preferred. To ensure the stability and convergence of the controller and reduce the fuel consumption, the switching conditions are optimized using the genetic algorithm. The detailed design steps of the coordinated controllers are described in the following section.

10.2.1 Parameter Identification

The inertia matrix and centroid position of the postcapture combination system are unknown, but they are necessary for the attitude controller design. Therefore these parameters are identified according to the following steps.

Combining Eqs. (10.10) and 10.15), we have

$$\boldsymbol{J}\dot{\boldsymbol{\omega}}_e = -\boldsymbol{\omega}^{\times}\boldsymbol{J}\boldsymbol{\omega} - \boldsymbol{J}\boldsymbol{R}\dot{\boldsymbol{\omega}}_d + \boldsymbol{T}_c + (\boldsymbol{R}\boldsymbol{F}) \times \boldsymbol{d} \tag{10.20}$$

where $\boldsymbol{F} = -\dfrac{[x, y, z]^T + \boldsymbol{R}^{-1}\boldsymbol{d}}{\left\|[x, y, z]^T + \boldsymbol{R}^{-1}\boldsymbol{d}\right\|}F_l$ is the tether tension vector, the tether tension F_l is measurable. According to the gripper's measurable centroid position, the capture position $[x, y, z]^T + \boldsymbol{R}^{-1}\boldsymbol{d}$ can be obtained. Assume the relative position between the platform and the gripper can be measured in very high accuracy, which is a few centimeters at least for the case of hundreds meters of distance.

Assume that the centroid position and the capture position in the combination body frame are $\Delta\boldsymbol{d}$ and $\boldsymbol{d}_0$, respectively, and the following relation can be obtained:

$$\boldsymbol{d} = \boldsymbol{d}_0 - \Delta\boldsymbol{d} \tag{10.21}$$

Eq. (10.20) can be written as:

$$\boldsymbol{J}\dot{\boldsymbol{\omega}}_e + \boldsymbol{\omega}^{\times}\boldsymbol{J}\boldsymbol{\omega} + \boldsymbol{J}\boldsymbol{R}\dot{\boldsymbol{\omega}}_d + (\boldsymbol{R}\boldsymbol{F})^{\times}\Delta\boldsymbol{d} = \boldsymbol{T}_c + (\boldsymbol{R}\boldsymbol{F})^{\times}\boldsymbol{d}_0 \tag{10.22}$$

The parameters to be identified are:

$$\boldsymbol{\theta} = (J_{11}\ \ J_{12}\ \ J_{13}\ \ J_{21}\ \ J_{22}\ \ J_{23}\ \ J_{31}\ \ J_{32}\ \ J_{33}\ \ \Delta d_1\ \ \Delta d_2\ \ \Delta d_3)^T$$

Eq. (10.22) could be rewritten in the following form:

$$\boldsymbol{T} = \Phi\boldsymbol{\theta} \tag{10.23}$$

where $\boldsymbol{T} = \boldsymbol{T}_c + (\boldsymbol{RF})^{\times}\boldsymbol{d}_0$, $\Phi = \begin{pmatrix} \Phi_1 \\ \Phi_2 \end{pmatrix}^T$,

$$\Phi_1 = \begin{pmatrix} \Phi_{11} & \omega_1\omega_3 & -\omega_1\omega_2 \\ \Phi_{21} & \omega_2\omega_3 & -{\omega_2}^2 \\ \Phi_{31} & {\omega_3}^2 & -\omega_2\omega_3 \\ -\omega_1\omega_3 & \Phi_{24} & {\omega_1}^2 \\ -\omega_2\omega_3 & \Phi_{25} & \omega_1\omega_2 \\ {\omega_3}^2 & \Phi_{26} & \omega_1\omega_3 \\ \omega_1\omega_2 & -{\omega_1}^2 & \Phi_{37} \\ {\omega_2}^2 & -\omega_1\omega_2 & \Phi_{38} \\ \omega_2\omega_3 & -\omega_1\omega_3 & \Phi_{39} \end{pmatrix}^T, \quad \Phi_2 = \left((\boldsymbol{RF})^{\times}\right)^T.$$

The elements of $\boldsymbol{\Phi}_1$ are as follows:

$$\begin{cases} \Phi_{11} = \Phi_{24} = \Phi_{37} = \dot{\omega}_{e1} + R_{11}\dot{\omega}_{d1} + R_{12}\dot{\omega}_{d2} + R_{13}\dot{\omega}_{d3} \\ \Phi_{21} = \Phi_{25} = \Phi_{38} = \dot{\omega}_{e2} + R_{21}\dot{\omega}_{d1} + R_{22}\dot{\omega}_{d2} + R_{23}\dot{\omega}_{d3} \\ \Phi_{31} = \Phi_{26} = \Phi_{39} = \dot{\omega}_{e3} + R_{31}\dot{\omega}_{d1} + R_{32}\dot{\omega}_{d2} + R_{33}\dot{\omega}_{d3} \end{cases}$$

Assume that the angular velocity ω and the angular acceleration $\dot{\omega}_e$ of the parameter matrix can be measured using a gyro compass. The value of $\boldsymbol{\sigma}_e$ can be obtained visually; therefore, $\boldsymbol{R}_{lp}$, $\boldsymbol{R}_{bl}$, and $\boldsymbol{R}$ can be acquired indirectly via computation. Also, the inputs $\boldsymbol{T}_c$ and $\boldsymbol{T}_l$ are known and available.

The formulations of the identification based on the least-squares method are:

$$\begin{cases} \hat{\boldsymbol{\theta}}(k) = \hat{\boldsymbol{\theta}}(k-1) + \boldsymbol{K}(k)\left[\gamma(k) - \boldsymbol{\Phi}(k)\hat{\boldsymbol{\theta}}(k-1)\right] \\ \boldsymbol{K}(k) = \boldsymbol{P}(k-1) + \Phi^T(k)\left[I + \boldsymbol{\Phi}(k)\boldsymbol{P}(k-1)\boldsymbol{\Phi}^T(k)\right]^{-1} \\ \boldsymbol{P}(k) = [I - \boldsymbol{K}(k)\Phi(k)]\boldsymbol{P}(k-1) \end{cases} \tag{10.24}$$

The identification algorithm is implemented according to the following steps:

(1) Set the initial values of $\hat{\boldsymbol{\theta}}(k)$ and $\boldsymbol{P}(k-1)$.
(2) Obtain the required sampled data, including ω, $\dot{\omega}_e$, $\boldsymbol{T}_c$, $\boldsymbol{T}_l$.
(3) Calculate $\boldsymbol{K}(k)$, $\hat{\boldsymbol{\theta}}(k)$, and $\boldsymbol{P}(k)$ using Eq. (10.24).
(4) Set $k = k+1$ and return to step (2) until the simulation is terminated.

10.2.2 Coordinated Controller of Tether and Thrusters

The tether tension could provide two axes of torques to control the pitch angle θ_e and the yaw angle ψ_e. However, only the variable F_l is available for the controller design. Hence, for a convenient controller design, we must

find a single variable to denote both the pitch and yaw angles. As shown in Fig. 10.1, when the attitude error, θ_e and ψ_e, are eliminated, the capture position vector $\boldsymbol{d}$ and the tether tension vector $\boldsymbol{F}$ will be collinear. Therefore the variable corresponding to the pitch and yaw angles could be the angle between $\boldsymbol{d}$ and $\boldsymbol{F}$, which is defined as η and given by:

$$\eta = \arccos\left(\frac{\boldsymbol{F}^T(\boldsymbol{R}^{-1}\boldsymbol{d})}{|\boldsymbol{F}||\boldsymbol{R}^{-1}\boldsymbol{d}|}\right) \tag{10.25}$$

The PD controller is adopted to control the pitch and yaw motions via η. The tether tension vector $\boldsymbol{F}$ could be measured, $\boldsymbol{R}$ could be computed from the attitude, and the value of $\boldsymbol{d}$ could be determined as identified in Section 10.2.1; therefore the value of η is available. The tether tension is given by

$$F_l = \begin{cases} (k_{pl} + k_{dl}S)\eta & (k_{pl} + k_{dl}S)\eta \geq 0 \\ 0 & (k_{pl} + k_{dl}S)\eta < 0 \end{cases} \tag{10.26}$$

where k_{pl} and k_{dl} denote the proportional and damping coefficients. The tether tension, F_l, must be positive.

By combining Eqs. (10.13) and (10.15), the control torque $\boldsymbol{T}_l$ can be obtained:

$$\boldsymbol{T}_l = \left[\boldsymbol{R}\left(\frac{[x, y, z]^T + \boldsymbol{R}^{-1}\boldsymbol{d}}{\left|\left|[x, y, z]^T + \boldsymbol{R}^{-1}\boldsymbol{d}\right|\right|}F_l\right)\right] \times \boldsymbol{d} \tag{10.27}$$

Only two axes of attitude torque can be provided by the space tether, which means that the left roll motion could only be controlled by the thruster force. Also, the roll motion exerts too great an influence on the other two motions, so the PD controller is adopted to stabilize the roll motion.

$$\boldsymbol{T}_c(1) = k_{pc}\phi_e + k_{dc}\omega_{ex} \tag{10.28}$$

The terms θ_e and ψ_e can be obtained from Eqs. (10.7) and (10.8), and k_{pc} and k_{dc} denote the proportional coefficient and the damping coefficient.

As a result, the coordinated controller of the tether tension and the thruster force is obtained in Eqs. (10.26) and (10.28).

10.2.3 Thruster Controller Design

When the pitch and yaw error attitude are controlled within a certain range, the controller is switched to the thruster control only. Though an inertia

matrix is acquired by the parameter identification, the errors of the identified variables exist, which can lead to instability in the control system. The sliding mode control approach is recognized as an efficient tool for design robust controllers for nonlinear dynamic plants under uncertainty conditions. Therefore sliding mode control is adopted to deal with the uncertainty in the inertial matrix and other disturbances.

The error attitude dynamic equation is given by Eq. (10.10). The sliding surface is defined as $\boldsymbol{s}=\boldsymbol{\omega}_e+c\boldsymbol{\sigma}_e$, where $c>0$. The sliding mode controller is designed as:

$$\boldsymbol{T}_c=\boldsymbol{\omega}^{\times}\boldsymbol{J}\boldsymbol{\omega}+\boldsymbol{J}\dot{\boldsymbol{\omega}}_d-c\boldsymbol{J}G(\sigma_e)\boldsymbol{\omega}_e-\lambda\,\mathrm{sgn}(\boldsymbol{s}) \tag{10.29}$$

with $\lambda>0$.

Choose $V=\frac{1}{2}\boldsymbol{s}^T\boldsymbol{J}\boldsymbol{s}$ as the Lyapunov function, and the time derivative of V is:

$$\begin{aligned}\dot{V}&=\boldsymbol{s}^T\boldsymbol{J}\dot{\boldsymbol{s}}\\&=\boldsymbol{s}^T\boldsymbol{J}(\dot{\boldsymbol{\omega}}_e+c\dot{\boldsymbol{\sigma}}_e)\end{aligned} \tag{10.30}$$

By substituting Eq. (10.10) into (10.14), we have:

$$\begin{aligned}\dot{V}&=\boldsymbol{s}^T(\boldsymbol{T}_c-\boldsymbol{\omega}^{\times}\boldsymbol{J}\boldsymbol{\omega}-\boldsymbol{J}\dot{\boldsymbol{\omega}}_d+c\boldsymbol{J}G(\boldsymbol{\sigma}_e)\boldsymbol{\omega}_e)\\&=\boldsymbol{s}^T[-\lambda\,\mathrm{sgn}(\boldsymbol{s})+f(\Delta\boldsymbol{J})]\end{aligned}$$

where $f(\Delta\boldsymbol{J})=-\boldsymbol{\omega}^{\times}\Delta\boldsymbol{J}\boldsymbol{\omega}-\Delta\boldsymbol{J}\dot{\boldsymbol{\omega}}_d+\Delta\boldsymbol{J}G(\boldsymbol{\sigma}_e)\boldsymbol{\omega}_e$. The term $\Delta\boldsymbol{J}$, which is due to the fuel consumption, is bounded, implying that $f(\Delta\boldsymbol{J})$ is also bounded. Assume $\begin{cases}\Delta_{\max}=\|f(\Delta\boldsymbol{J})\|_{\infty}\\ f(\Delta\boldsymbol{J})=[\Delta_1\ \ \Delta_2\ \ \Delta_3]^T\end{cases}$ and setting $\lambda=\Delta_{\max}+\delta$ in which δ is an arbitrary positive number, one can derive:

$$\begin{aligned}\dot{V}&=\sum_{i=1}^{3}\boldsymbol{s}_i^T[-(\Delta_{\max}+\delta)\,\mathrm{sgn}(\boldsymbol{s}_i)+\Delta_i]\\&=\sum_{i=1}^{3}\boldsymbol{s}_i^T[-\delta\,\mathrm{sgn}(\boldsymbol{s}_i)-\Delta_{\max}\,\mathrm{sgn}(\boldsymbol{s}_i)+\Delta_i]\\&=-\sum_{i=1}^{3}\boldsymbol{s}_i^T\delta\,\mathrm{sgn}(\boldsymbol{s}_i)+\sum_{i=1}^{3}[-\Delta_{\max}\boldsymbol{s}_i^T\,\mathrm{sgn}(\boldsymbol{s}_i)+\Delta_i\boldsymbol{s}_i^T]\\&\le-\sum_{i=1}^{3}\boldsymbol{s}_i^T\delta\,\mathrm{sgn}(\boldsymbol{s}_i)\\&\le 0\end{aligned}$$

$V > 0$ and $V \leq 0$, so it is believed that asymptotically stable system meets the sliding condition.

There must be chattering in the control system for the existence of the sign function in Eq. (10.29). To solve this problem, the saturation functions is used instead:

$$sat(s_i, \varepsilon) = \begin{cases} 1 & s_i > \varepsilon \\ s_i/\varepsilon & -\varepsilon \leq s_i \leq \varepsilon \\ -1 & s_i < -\varepsilon \end{cases} \tag{10.31}$$

where $i = 1,2,3$ and ε is a positive number.

10.2.4 Switching Conditions and Parameter Optimization

When using the tether tension to control the pitch ψ and yaw θ angles, one expects to make full use of the tether tension when ψ and θ are both relatively large, and to utilize the thruster force to stabilize the angles and achieve high attitude control accuracy when they are relatively small. Therefore the pitch angle ψ and the yaw angle θ are chosen as the switching conditions of the coordinated controller and the thruster controller only. The switching conditions are given by:

$$\begin{cases} |\psi| \leq \psi_s \\ |\theta| \leq \theta_s \end{cases} \tag{10.32}$$

where ψ_s and θ_s are the switching angles and are both subject to constants. When the conditions in Eq. (10.32) are satisfied, Eq. (10.24) is utilized. In contrast, when any one of these conditions is not satisfied, Eqs. (10.22) and (10.23) are utilized.

The angles ψ_s and θ_s have remarkable effects on the coordinated control performance. Thus one expects to find the optimal values of ψ_s and θ_s, which can optimize performance of the control index. The optimization of ψ_s and θ_s is actually a problem of optimization with constraints because the optimal values should enable the system to work with the lowest possible fuel consumption, whereas the constraints on the control input should always be satisfied. This parameter optimization problem could not be solved in an analytical way, for it does not work with an attitude tracking control problem because of its complexity. The genetic algorithm should be resorted to solve this constraint-submitted nonlinear parameter optimization problem. In this case, an index for evaluating the performance of the system is defined as follows:

$$J_1 = k_1 \int_0^{t_f} \boldsymbol{T}_c^T \boldsymbol{T}_c dt + k_2 \int_0^{t_f} F^T F dt + k_3 \int_0^{t_f} \boldsymbol{\sigma}_e^T \boldsymbol{\sigma}_e dt \tag{10.33}$$

where the first term of the right side is the weighted fuel consumption, the second is the weighted position influence of the tether tension for the combination system and the third is the penalty term, which can enhance the convergence speed and guarantee the stability of the combination system. However, improper switch values of the angles ψ_s and θ_s can lead to instability of the system. The terms k_1, k_2, and k_3 are their weights.

The genetic algorithm is realized in the following steps [23]:

(1) Choose search sets for both ψ_s and θ_s, encode them as n-bit binary strings, and generate the initial population with N_p individuals.

(2) Calculate the fitness value for each individual according to Eq. (10.28).

(3) From the current population, select the strings with probabilities proportional to their fitness values.

(4) The single-point crossover operation is performed on the selected strings with a probability of P_x.

(5) A mutation is then applied to the new chromosomes with a set probability of P_m. The new generation has now been completed.

(6) Evaluate the new generation using Eq. (10.28), and repeat Steps (3)–(6) until N_g generations are achieved.

Fig. 10.2 shows the block diagram of the coordinated attitude controller for the tethered space robot-target combination.

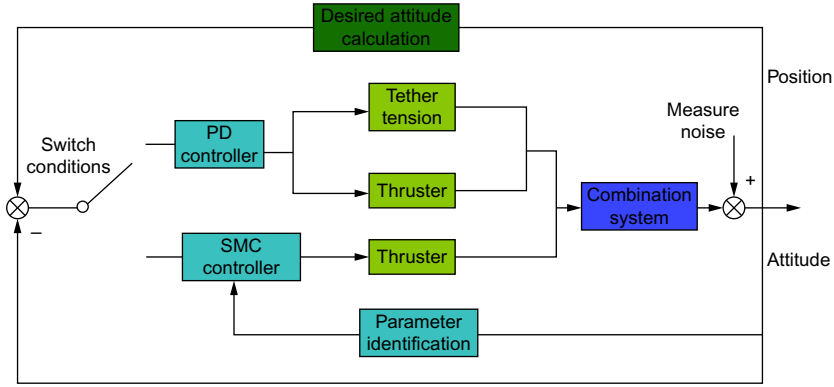

Fig. 10.2 Block diagram of the coordinated controllers.

10.3 NUMERICAL SIMULATION

In this section, simulation of the coordinated controller and the traditional thruster controller (the sliding mode controller of the thruster force only) are both carried out for comparison. Assume that the initial position of the combination is (200, 0, 0) m, the initial angular velocities of the three axes of the combination are all 10 degrees/s. Thrusters are assumed to have a constant control torque of 5 Nm when the corresponding thrusters are turned on and work in the PWM mode with a control cycle of 250 ms. Table 10.1 shows the initial values of the parameters.

Fig. 10.3 is the optimization result for J_1. It can be seen that J_1 converges at 567.5 after 17 generations. As shown in Table 10.2, the optimal values of the switching condition are $\psi_s = 29.23$ degrees, $\theta_s = 11.85$ degrees.

Table 10.1 Initial value of the parameters

Parameters	Initial values	Parameters	Initial values
$\boldsymbol{\sigma}_e$	(0.0999,0.2015,0.1008)	$\boldsymbol{\omega}_e$	(10,10,10) degrees/s
c	1	$(x \ \ y \ \ z)^T$	(200,0,0)m
$(\dot{x} \ \ \dot{y} \ \ \dot{z})^T$	(0,0,0)m/s	n	0.0011 rad/s

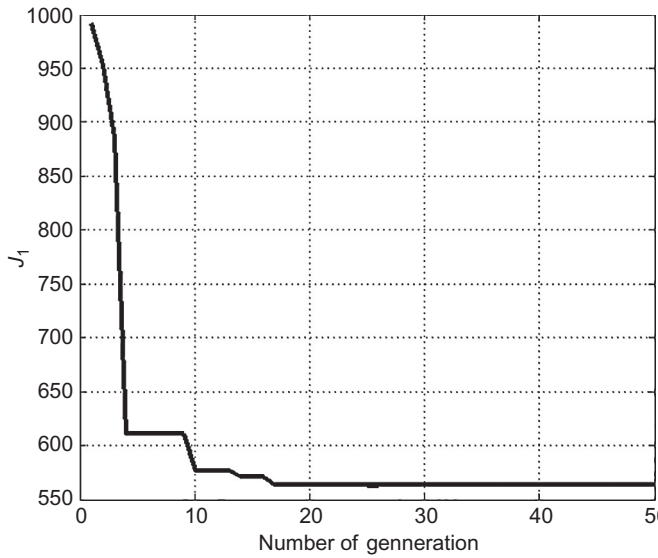

Fig. 10.3 Value of J_1 with respect to the number of generation.

Table 10.2 Optimal values of switching conditions

Parameters	Optimal values	Parameters	Optimal values
ψ_s	29.23 degrees	θ_s	11.85 degrees

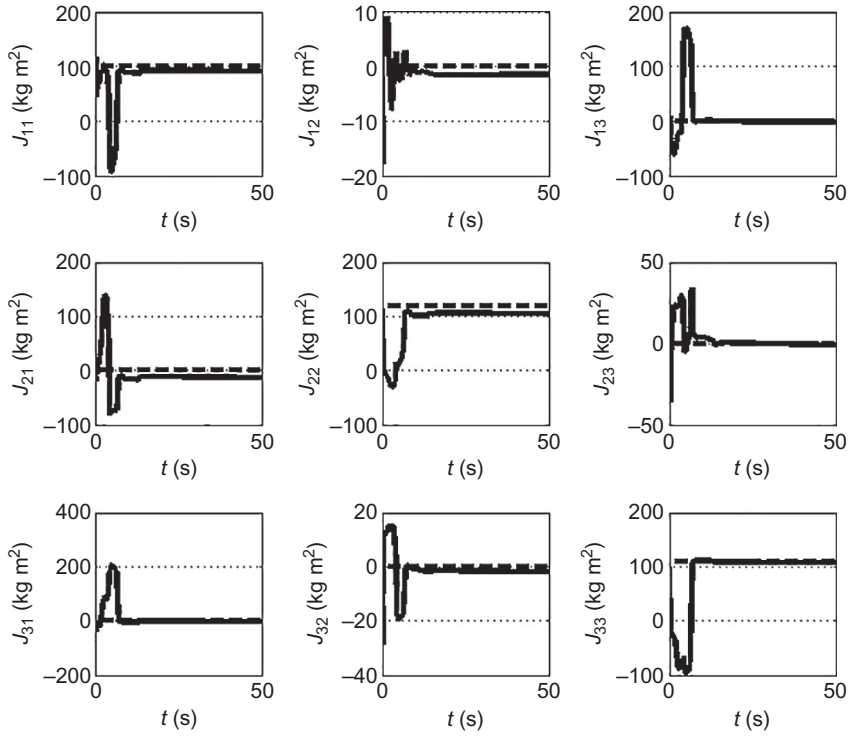

Fig. 10.4 Identification value of J with respect to time.

Fig. 10.4 shows the identification results of the inertial matrix J. The maximum identification errors of $\boldsymbol{J}_{11}$, $\boldsymbol{J}_{22}$, and $\boldsymbol{J}_{33}$ are 7.10%, 8.79%, and 2.54%, respectively, which are less than 10%. Moreover, the maximum identification error is 12.1 kg m^2 of $\boldsymbol{J}_{21}$. As indicated in Fig. 10.5, the actual value of Δd is (0, 0, 0) m and the identified values (−0.24, 0.06, 0.11) m.

Figs. 10.6 and 10.7 provide the simulation results of the three-axis attitude σ_e and the corresponding Euler angles (1-2-3). From Figs. 10.6 and 10.7, one can be see that the convergence time of the coordinated controller is about 35 s, which is 10 s longer than that of the controller of thrusters only. Because the tether could provide greater torque control, the pitch θ_e and yaw ψ_e angles could be controlled in a shorter time during the initial stage

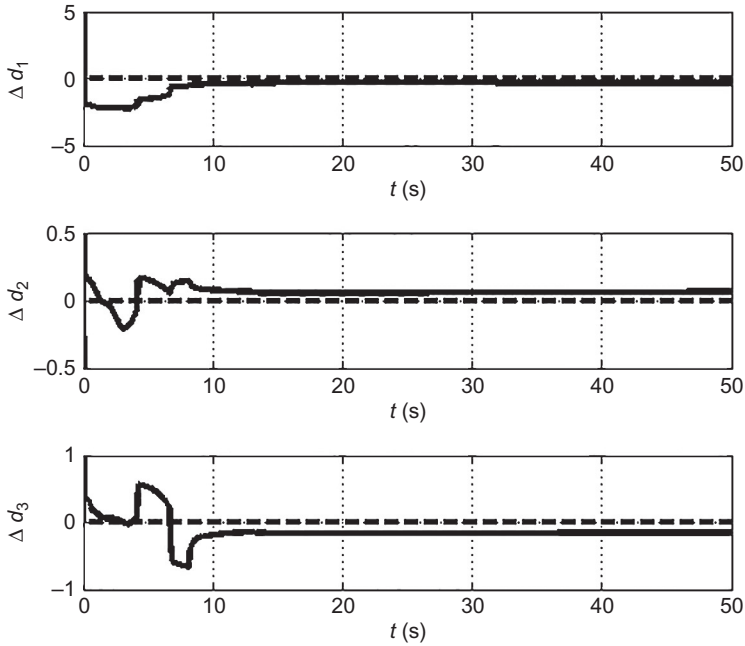

Fig. 10.5 Identification value of Δd with respect to time.

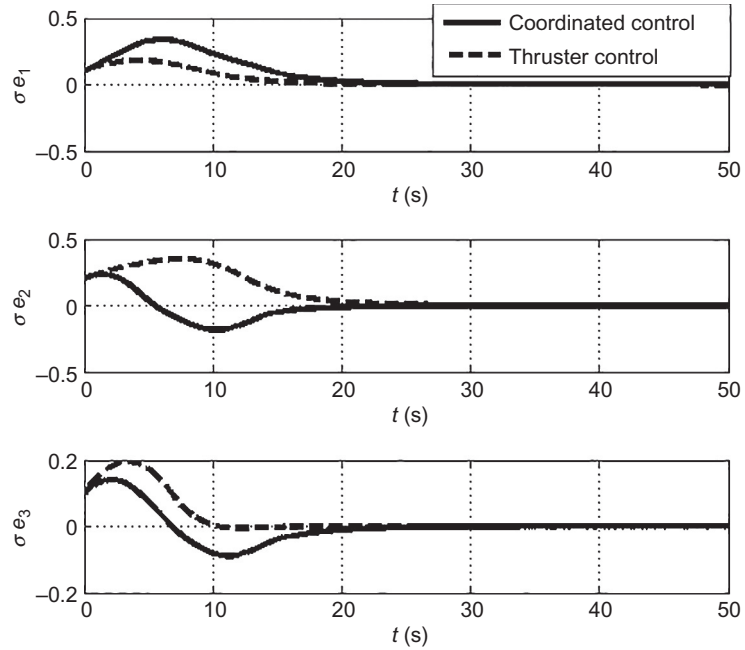

Fig. 10.6 Three-axis attitude $\boldsymbol{\sigma}_e$.

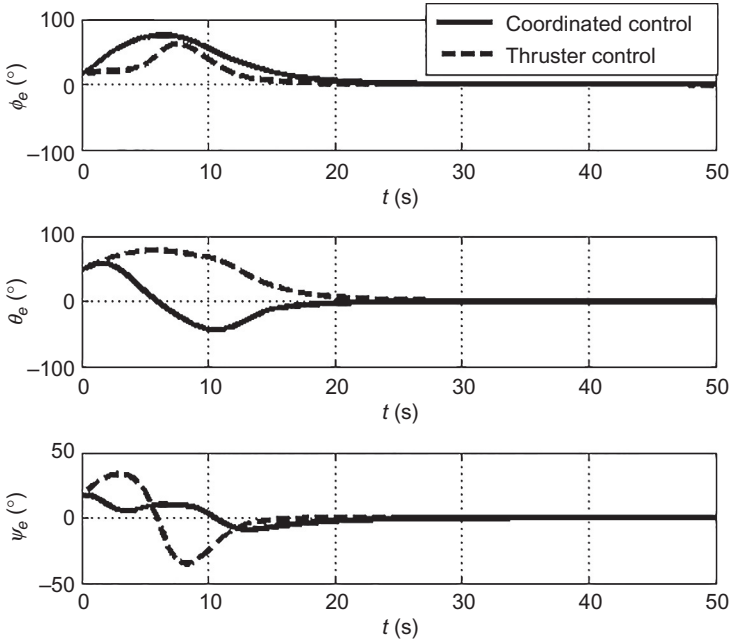

Fig. 10.7 Euler angles of three-axis attitude.

and the maximum amplitudes of θ_e and ψ_e of the coordinated controller are -43.5 degrees and -15.8 degrees, respectively. However, the maximum amplitudes of θ_e and ψ_e for the thruster controller only are 78.5 degrees and -35.1 degrees. An angle of 78.5 degrees may lead to an entanglement of the tether with the combination and cause instability in the space platform and the entire system, which must be avoided. This result clearly suggests that the use of the coordinated controller of the tether and thrusters can lead to smaller amplitudes of the pitch ψ and yaw θ angles and lower the possibility of the entanglement of the tether with the combination.

An entanglement of the tether usually results from the pitch and yaw angles. However, this finding does not mean that the roll motion can change freely without any control because the three-axis attitudes are coupled and the roll motion exerts an influence on the other two motions. The results of a PD controller for the roll motion are provided in Fig. 10.7. Fig. 10.8 shows the three-axis angular velocities of the coordinated controller and the thruster controller only. The maximum value of η in Fig. 10.9 is 58.6 degrees, which is relatively safe to the combination system, because the entanglement of the tether is more likely to occur when $\eta > 90$ degrees.

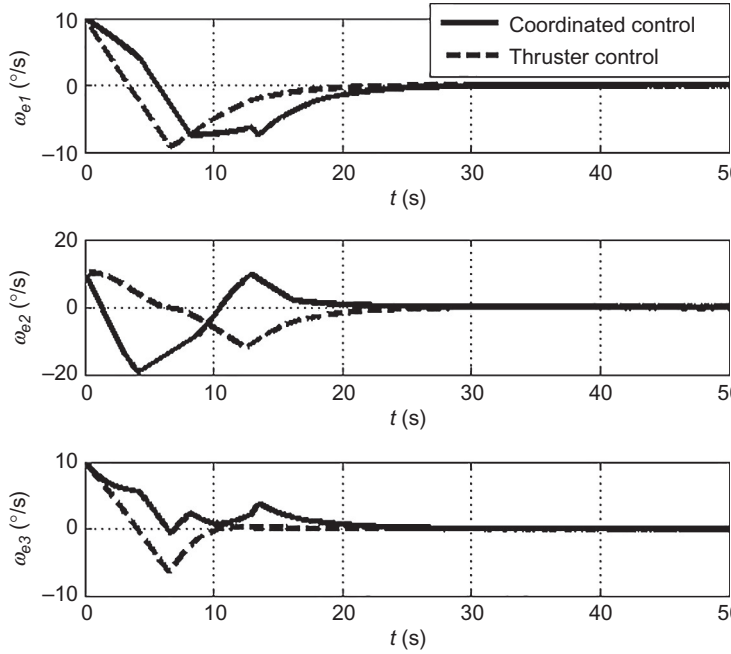

Fig. 10.8 Three-axis angular velocity.

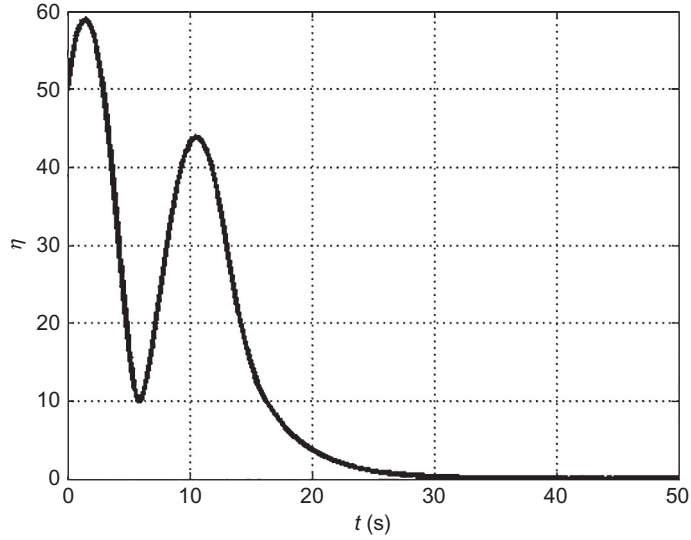

Fig. 10.9 Angle of η.

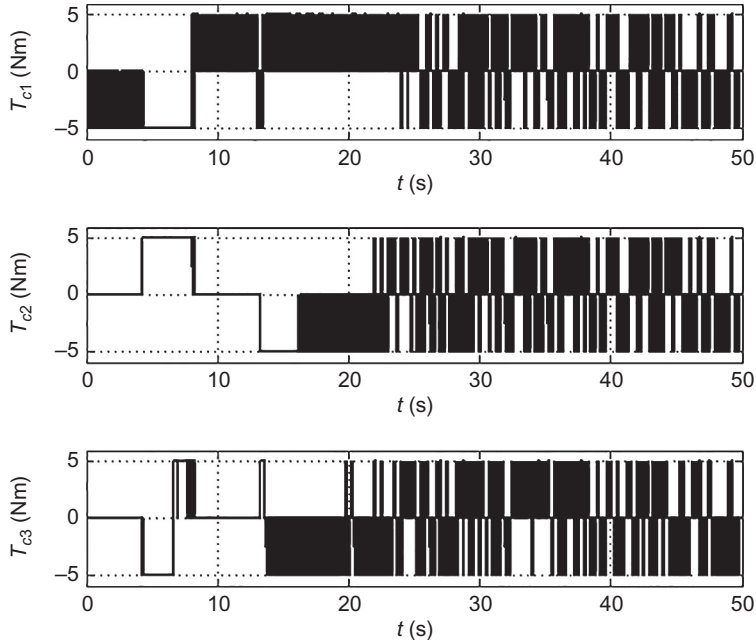

Fig. 10.10 Control commands of thrusters for coordinated control.

A comparison between the coordinated control of the tether and thrusters and the control of thrusters can be observed in Figs. 10.10 and 10.11. The second and the third elements of $\boldsymbol{T}_c$ become zero 2 times, and the overall control torques of the coordinated control are clearly smaller than that of the thruster control. Figs. 10.12 and 10.13 demonstrate that the tether tension is utilized for two times and that the maximum torque control of the tether is approximately 18.3 Nm, which is three times bigger than that of the thruster control and could effectively lower the attitude amplitudes of the combination as shown in Figs. 10.7 and 10.8.

The fuel consumption function is defined as follows:

$$M = \int_0^{t_f} \boldsymbol{T}_c^T \boldsymbol{T}_c dt \tag{10.34}$$

Fig. 10.14 compares the fuel consumption of the coordinated control and the thruster control. The fuel consumption of the coordinated control consists of two parts: one part is the fuel consumption required to control the roll motion when the coordinated controller is applied, and the other part is the fuel consumption of the thruster controller when the switching

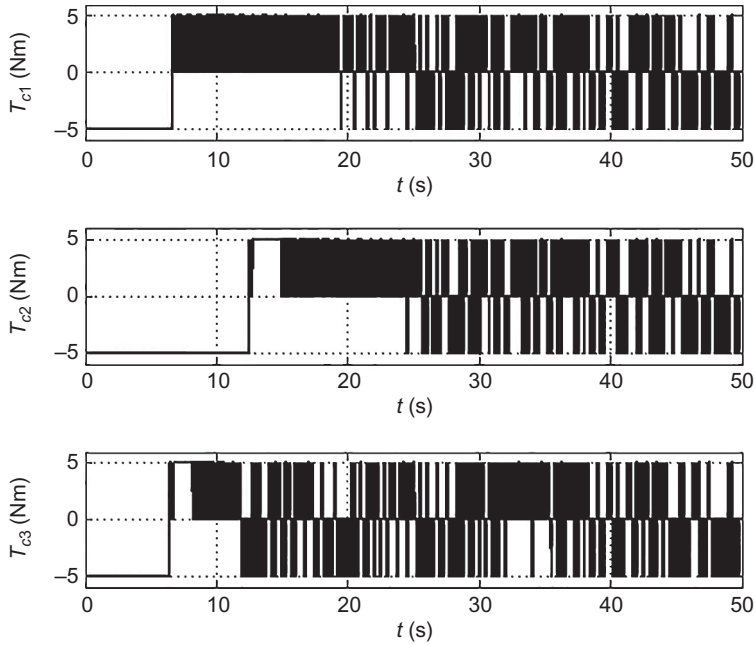

Fig. 10.11 Control commands of thrusters for traditional thruster control.

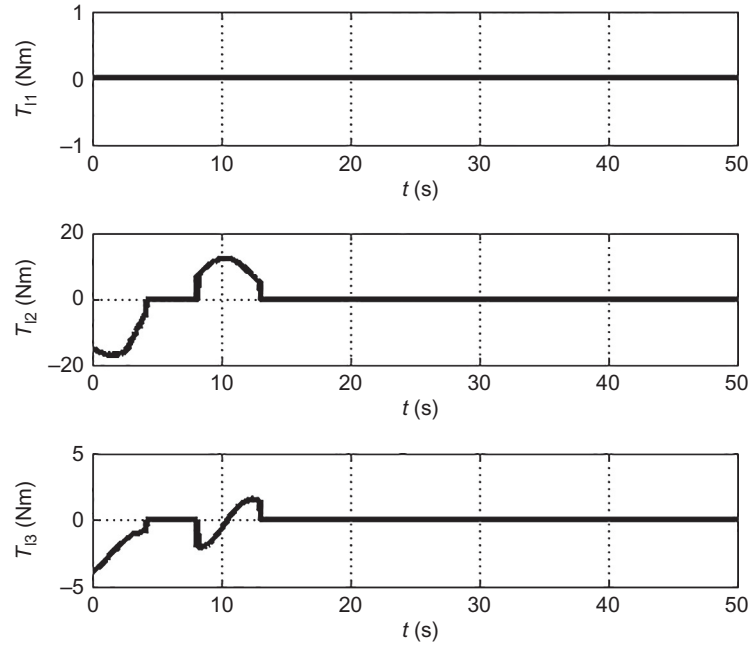

Fig. 10.12 Torques of tether tension.

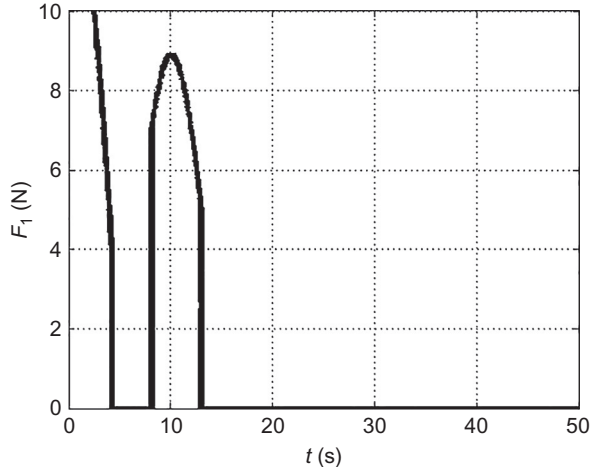

Fig. 10.13 Tether tension.

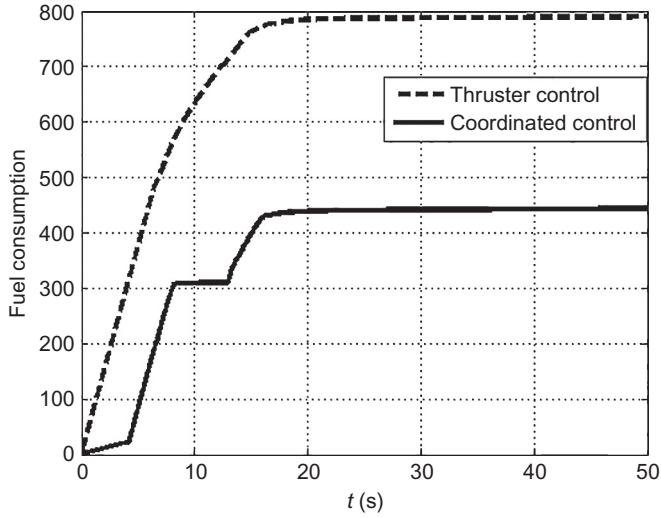

Fig. 10.14 Comparison of the fuel consumption.

conditions (Eq. 10.19) are satisfied. The final fuel consumption of the coordinated control is 486, while that of the thruster control is approximately 61.5% higher at 785, which clearly demonstrates that the coordinated control could efficiently reduce the fuel consumption.

Figs. 10.15 and 10.16 indicate the influence of the tether tension on the combination position and the linear velocity. One can see that the

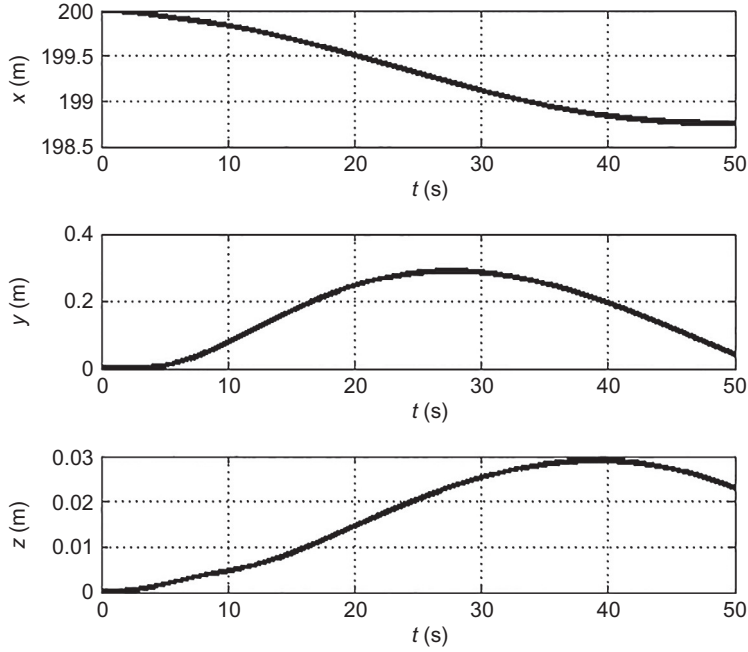

Fig. 10.15 Position changes due to the tension.

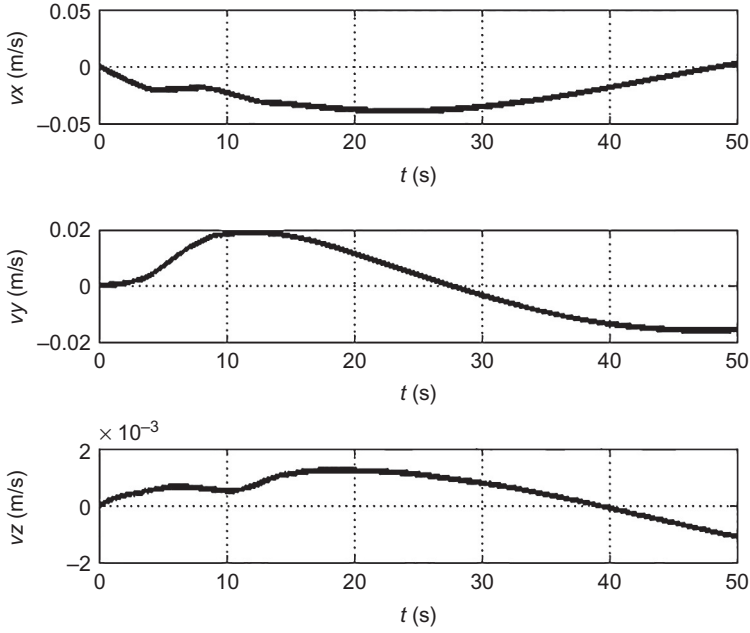

Fig. 10.16 Linear velocity changes due to the tension.

displacement due to the tether tension is (2.300, 0.001, 0.100) m, and the velocity change is (0.005, − 0.018, 0) m/s, which are acceptable values for postcapture attitude control.

REFERENCES

[1] M. Nohmi, T. Yamamoto, Y. Takagi, Microgravity experiment for attitude control of a tethered body by arm link motion, in: IEEE International Conference on Mechatronics and Automation, 2007 (ICMA 2007), 2007.

[2] M. Nohmi, Attitude control of a tethered space robot by link motion under microgravity, in: Proceedings of the 2004 IEEE International Conference on Control Applications, vol. 1, IEEE, 2004.

[3] M. Nohmi, Mission design of a tethered robot satellite "STARS" for orbital experiment, in: 2009 IEEE Control Applications (CCA) & Intelligent Control (ISIC), 2009.

[4] Godard, K.D. Kumar, B. Tan, Nonlinear optimal control of tethered satellite systems using tether offset in the presence of tether failure, Acta Astronaut. 66 (9) (2010) 1434–1448.

[5] K.D. Kumar, K. Kumar, Satellite pitch and roll attitude maneuvers through very short tethers, Acta Astronaut. 44 (5) (1999) 257–265.

[6] P.B. Beda, On requirements for attitude dynamics and stability control for tethered satellite systems, JSME Int. J. Ser. C 43 (3) (2000) 678–683.

[7] O. Mori, S. Matunaga, Formation and attitude control for rotational tethered satellite clusters, J. Spacecr. Rocket. 44 (1) (2007) 211–220.

[8] I. Chang, S.-Y. Park, K.-H. Choi, Nonlinear attitude control of a tether-connected multi-satellite in three-dimensional space, IEEE Trans. Aerosp. Electron. Syst. 46 (4) (2010) 1950–1968.

[9] C. Menon, C. Bombardelli, Self-stabilising attitude control for spinning tethered formations, Acta Astronaut. 60 (10) (2007) 828–833.

[10] S. Bergamaschi, F. Bonon, Coupling of tether lateral vibration and subsatellite attitude motion, J. Guid. Control. Dyn. 15 (5) (1992) 1284–1286.

[11] K. Yoshida, D. Dimitrov, H. Nakanishi, On the capture of tumbling satellite by a space robot, in: 2006 IEEE/RSJ International Conference on Intelligent Robots and Systems, IEEE, 2006.

[12] A. Flores-Abad, O. Ma, Control of a space robot for minimal attitude disturbance to the base satellite for capturing a tumbling satellite, in: SPIE Defense, Security, and Sensing, International Society for Optics and Photonics, 2012.

[13] S. Liu, L. Wu, Z. Lu, Impact dynamics and control of a flexible dual-arm space robot capturing an object, Appl. Math. Comput. 185 (2) (2007) 1149–1159.

[14] T.-C. Nguyen-Huynh, I. Sharf, Adaptive ReactionLess motion with joint limit avoidance for robotic capture of unknown target in space, in: 2012 IEEE/RSJ International Conference on Intelligent Robots and Systems (IROS), IEEE, 2012.

[15] F. Aghili, Optimal control of a space manipulator for detumbling of a target satellite, in: IEEE International Conference on Robotics and Automation, 2009 (ICRA'09), IEEE, 2009.

[16] F. Aghili, Coordination control of a free-flying manipulator and its base attitude to capture and detumble a noncooperative satellite, in: IROS 2009IEEE/RSJ International Conference on Intelligent Robots and Systems, 2009, IEEE, 2009.

[17] W. Xu, et al., Target berthing and base reorientation of free-floating space robotic system after capturing, Acta Astronaut. 64 (2) (2009) 109–126.

[18] Y. Nakamura, F. Sasaki, S. Nakasuka, Guidance and control of tethered retriever with collaborative tension-thruster control for future on-orbit service missions, in: Proceedings of the 8th International Symposium on Artificial Intelligence, Robotics and Automation in Space (i-SAIRAS 2005), 2005.
[19] S. Hokamoto, N. Imamura, V.J. Modi, Dynamics and control of a tethered space robot with tension, Adv. Astronaut. Sci. 109 (2002) 1587–1595.
[20] K.K. Mankala, S.K. Agrawal, Dynamic modeling and simulation of satellite tethered systems, J. Vib. Acoust. 127 (2) (2005) 144–156.
[21] J.L. Crassidis, F.L. Markley, Sliding mode control using modified Rodrigues parameters, J. Guid. Control. Dyn. 19 (6) (1996) 1381–1383.
[22] G.Q. Xing, S.A. Parvez, Nonlinear attitude state tracking control for spacecraft, J. Guid. Control. Dyn. 24 (3) (2001) 624–626.
[23] M. Srinivas, L.M. Patnaik, Genetic algorithms: a survey, Computer 27 (6) (1994) 17–26.